Effects of Aging, Temperature and Frequency Dependent Properties of Asphalt Concrete on Top-Down Cracking

Mohsen Alae[1]; Yanqing Zhao[2]; Zhen Leng[3]

[1]Research Assistant, School of Transportation Engineering, Dalian University of Technology, Dalian 116024, China. Email: mohsen_374@yahoo.com

[2]Professor, Ph.D., School of Transportation Engineering, Dalian University of Technology, Dalian 116024, China. Email (corresponding author): yanqing_zhao@dlut.edu.cn

[3]Associate Professor, Department of Civil and Environmental Engineering, The Hong Kong Polytechnic University, Hung Hom, Kowloon, Hong Kong. Email: zhen.leng@polyu.edu.hk

Abstract: The horizontal tensile strain at the top of asphalt concrete (AC) layer is considered as the most appropriate response of pavement for analyzing Top-down cracking (TDC). In this study, influence of vehicle speed, temperature and non-uniform aging modulus on TDC are explored according to tensile strain magnitudes at the pavement surface. Utilizing a new analysis approach, the responses are computed at top and bottom of thick and thin AC layers in pavements with cement-treated base (CTB) and granular base (GB). The results demonstrate that critical tensile strain arises at the top of AC layer and in transverse direction. Variations of speed at low temperature affect the critical type of cracking, while at intermediate and elevated temperatures TDC is dominant at all speeds analyzed. It is shown that modulus gradient induced by aging is an influencing factor in TDC which causes critical location of TDC to vary at the surface significantly.

Keywords: top-down cracking; aging; vehicle speed; horizontal strain; temperature; asphalt

pavement

1. Introduction

In computing the fatigue life of asphalt pavements and design procedures of flexible pavement structures, longitudinal strain at the bottom of asphalt layer is widely regarded as the critical strain. But new research works and field experiences have revealed that fatigue cracking could also initiate at the top of pavement and then propagate downwards (Gu et al. 2018; Chun et al. 2018; Alae et al. 2018; Wu et al. 2019). The longitudinal top-down fatigue cracking diminishes the pavement serviceability and increases water penetration into the layers which leads to pavement deterioration. Top-down cracking (TDC) is now well known as a prominent type of fatigue distress in flexible pavements. Several mechanistic-empirical (M-E) models were developed by researchers to characterize the TDC performance mechanistically and calibrated to field performance, and the TDC was found to be the first stage of fatigue cracking (Ling et al. 2019b; Dinegdae and Birgisson 2018).

There are several factors that affect the pavement responses when subjected to varying traffic loading and environmental conditions. Loading frequency is a crucial factor in time-dependent materials which affects the pavement responses and fatigue life significantly. Previous studies revealed that effects of vehicle speed on dynamic loads and pavement response are not identical (Perret and Dumont 2004; Qin et al. 2010; Rahman et al. 2019). In fact, different vehicle speeds will lead to various loading times on the asphalt pavement. Since the complex modulus of asphalt mixture depends on temperature and loading frequency, the asphalt pavement will respond differently in stiffness. According to the study conducted by Mikhail

and Mamlouk (1997), since the loading time at the speed of 20 km/h is longer, the vertical strain is almost 10 times larger than that at 130 km/h speed. Different researchers concluded that consideration of vehicle speed in mechanistic design of pavement is necessary (Lourens 1992; Siddharthan et al. 2002; Sarkar 2016). It is worthy to note that the field measurements conducted by Chatti et al. (1996) and Dai et al. (1997) confirmed that the measured strains at the mid-depth and bottom of asphalt layer decrease as the truck speed increases. Although, significant studies have been conducted on bottom-up fatigue cracking, the influence of vehicle speed at different temperatures on TDC was not studied widely.

Stiffness gradient due to aging is another factor which plays an important role in TDC (Ling et al. 2017a; Wang et al. 2013). Aging, is normally defined as change in the rheological properties of asphalt binders/mixtures due to variations in chemical composition during construction and its service life period. Aging induces the increase of stiffness at the pavement surface which leads to the decrease of fracture energy and consequently crack initiation (Al-Rub et al. 2013). In the study conducted by Ling et al. (2018), the LTPP data were utilized to develop mechanics-based prediction models to compute a TDC initiation energy parameter and crack initiation time. The recent studies showed that the long-term field aging of AC layer is non-uniform within the top 4 cm which causes the modulus to change nonuniformly with depth (Ling et al. 2017b). This finding was also indicated by Wambura et al. (1999) where in Kenya the severe age-hardening occurred just in the top few millimeters of the AC surface.

Once the air temperature increases or decreases, temperature at the bottom of asphalt layer needs more time to change in compare with that at the surface. Hence, considering non-uniform temperature gradient effect is necessary in TDC analysis and pavement design. Archilla (2015)

indicated that the inverse modulus gradient due to the high-temperature increases the likelihood of TDC. To consider the aforementioned factors effect on TDC based on mechanistic analyses, the TDC mechanism needs to be recognized.

Several types of responses have been nominated as the driving forces of TDC. Some researchers demonstrated that vertical shear strain at the tire edge could result in TDC (Mohammad et al. 2005; Wang et al. 2013). More than that, vertical tensile strain at the top AC layer has been also revealed as a cause of TDC (Kim et al. 2009; Roque et al. 2006). This finding is questionable since cracking is usually believed to be caused by stress or strain in the horizontal plane. The newly developed mechanistic-empirical pavement design guide (MEPDG) suggested that critical horizontal strain at the pavement surface is related to TDC (ARA, 2004). However, there are problems associated with the procedure used in the MEPDG for identifying the maximum tensile strain at the pavement surface. Accordingly, this research utilizes the horizontal tensile strains at top of asphalt layer for TDC evaluation.

Traditional multi-layered elastic analysis is not able to calculate horizontal strains at the pavement surface correctly and thus results in bottom-up cracking (Myers et al. 1998; Kim et al. 2009). The irregular oscillations of the integrand in analytical solution of a multi-layered elastic system cause the poor convergence to occur near the pavement surface, which may lead to large errors in response analysis (Blakemore et al. 1976; Sidi 1988; Zhao et al. 2015). To solve this problem successfully and calculate the surface responses precisely, Zhao et al. (2015) divided the integrand into regular low- and high-frequency components and accelerated the convergence.

2. Objectives

To demonstrate MEPDG may not be able to predict critical fatigue distress accurately, this study aims to identify the crack initiation location at the pavement surface and compare with analysis locations adopted in the MEPDG. Using the new analysis procedure, the critical horizontal strain as the major cause of TDC is calculated accurately and computation time decreases significantly. To increase the overall effectiveness of the research effort, a follow-up study is conducted by evaluating the effects of vehicle speed (loading frequency), non-uniform aging and temperature gradients as the influencing factors on TDC. This research provides beneficial insight to analysis and design of asphalt pavements and overlay from a mechanistic point of view.

3. Methodology

3.1. Layered Elastic Theory

Due to the complexity of TDC mode, M-E approach could be a reasonable approach to accurately describe the TDC occurring in asphalt pavements. The layered elastic theory (LET) has been extensively used in the M-E design to perform the pavement response analysis (Shell International Petroleum Company 1978; Asphalt Institute 1991; ARA 2004). For instance, the Burmister's solution for the horizontal radial stress in the *i*th layer is given by (Burmister 1943; Huang 2003):

$$R = q\alpha\int_0^\infty \left[J_0(m\rho)J_1(m\alpha) - \frac{J_1(m\rho)J_1(m\alpha)}{m\rho} \right] \begin{Bmatrix} \left[A_i + C_i(1+m\lambda)\right]e^{-m(\lambda_i-\lambda)} \\ +\left[B_i - D_i(1-m\lambda)\right]e^{-m(\lambda-\lambda_{i-1})} \\ +2\mu_i m J_0(m\rho)\left[C_i e^{-m(\lambda_i-\lambda)} - D_i e^{-m(\lambda-\lambda_{i-1})}\right] \end{Bmatrix} dm \quad (1)$$

where $\rho = r/H$ and $\lambda = z/H$; H is the distance from the surface to the upper boundary of the lowest layer; r and z are the cylindrical coordinates in radial and vertical directions; m is the

integration variable; J_0 and J_1 are the first kind of Bessel functions with order of zero and one, respectively. A_i, B_i, C_i and D_i are constants of integration of the ith layer. These constants are computed by the continuity and boundary conditions. α is the ratio of load radius to H and q is magnitude of the load.

In order to demonstrate the problem, a typical pavement including a 20 cm AC layer, a 40 cm granular base (GB) layer, and a subgrade have been analyzed. Geometry of the pavement with the analysis points "A" and "B" is shown in Figure 1. The layers moduli are 3000, 300 and 80 MPa, and Poisson's ratios are 0.3, 0.35 and 0.4, respectively. Figure 2 illustrates the integrand (function being integrated in the indefinite integral) in Equation (1) at the pavement surface (point A) and at mid-depth of AC layer (point B) which are located 3 cm far from the loading center at a radial distance. The figure shows that the complicated oscillatory behaviour of the integrand at the surface decays more slowly than that at a deeper depth. Accordingly, it is quite difficult to compute the results at the surface accurately.

3.2. Numerical Integration Algorithm

To solve complex irregular oscillating behavior of the integrand, an "integration then summation" procedure is generally effective in computing the integral (Davis and Rabinowitz 1988; Evans 1993). Once the integration converges gradually, an extrapolation technique is needed to accelerate the convergence (Sidi, 2003). This technique which is specified as the ISE approach, cannot be simply applied to the integral in Equation (1), because the oscillation caused by a product of two Bessel functions is very complicated.

Therefore, the Lucas algorithm which represents the product in equation above as the sum of two oscillating functions was utilized to effectively apply the ISE method to the integral

131 (Lucas 1995; Zhao et al. 2015). The complicated oscillating behaviour of the integrand at point
132 "A" illustrated in Figure 2 was converted to two simple oscillations by dividing the integrand
133 into low- and high-frequency components and depicted in Figure 3. The integration, summation
134 and extrapolation, (ISE) method was then utilized to efficiently analyze the integral.

135 By implementing the layered elastic solutions and the integration algorithm in the
136 computer code, the strain responses at the surface are calculated. The results obtained from this
137 analysis procedure were extensively verified with finite element method (FEM) and boundary
138 conditions, and accuracy of the new analysis procedures in determination of pavement
139 responses at the surface has been confirmed. Verification details of this approach were
140 presented elsewhere (Zhao et al. 2015).

141 In this study, the new analysis approach as mentioned previously was employed to compute
142 the horizontal strains at the surface of pavement and different transverse locations, ranging from
143 the center of the dual tires to a distance of 55 cm. The transverse locations analyzed at the
144 surface are depicted in Figures 4(*a* and *b*) for the thick and thin pavement structures,
145 respectively. To investigate the influence of vehicle speed, non-uniform aging and temperature
146 on TDC, the typical pavements with material properties listed in Table 1 were analyzed. The
147 table represents the thick pavement structure with a total AC layer thickness of 26 cm and a
148 base layer of 40 cm, as well as a thin pavement structure with a 10 cm AC layer and a 30 cm
149 base layer. For both thick and thin pavements, two different base layer types, granular base (GB)
150 and cement-treated base (CTB), were considered. In addition, the layers interfaces were
151 assumed fully-bonded in the analyses.

152 **3.3. Material Characterization**

153 Because of the time-temperature dependent behavior of asphalt mixture, dynamic modulus
154 master curve is used to describe the viscoelastic property of asphalt mixture by conducting
155 complex modulus test at various conditions. In this research, a stone mastic asphalt (SMA) and
156 two superpave mixtures were utilized with 12.5, 19 and 25 mm nominal maximum aggregate
157 size, respectively. For brevity, the three mixtures were abbreviated as SMA13, Sup20 and
158 Sup25, with asphalt contents of 4.1%, 4.3% and 4.5% respectively. The aggregate gradation of
159 the mixtures is presented in Table 2. A neat performance grade (PG) 64-22 binder was used for
160 Sup25 mixture, while an SBS-modified PG 76-22 binder was used for the SMA13 and Sup20
161 mixtures.

162 According to AASHTO TP 62-07 (AASHTO, 2007), dynamic moduli of the mixtures were
163 calculated at six frequencies (20, 10, 5, 1, 0.5 and 0.1 Hz) and temperatures (-10, 0, 15, 30, 40
164 and 55°C). In this study, the Modified Havriliak-Negami (MHN) Model is used to construct the
165 dynamic moduli master curves. The MHN model is given by:

166
$$E^*(i\omega_r) = E_0^* + \frac{E_\infty^* - E_0^*}{\left[1 + (\frac{\omega_0}{i\omega_r})^\alpha\right]^\beta} \quad (2)$$

167 where ω_r is reduced angular frequency; E_∞^* and E_0^* are complex moduli as ω_r approaches
168 ∞ and 0, respectively; ω_0 is related to the time-temperature shifting and controls the
169 horizontal positions of master curves, and α and β are model coefficients. According to the
170 time-temperature superposition principle (TTSP), ω_r and cyclic frequency, f, are related by
171 (Ferry 1980):

172
$$\omega_r = 2\pi f \alpha_T \quad (3)$$

173 where α_T is the time-temperature shift factor. The Williams-Landel-Ferry (WLF) equation in

174 Equation (4) is used to model α_T as a function of temperature T :

175 $$\log \alpha_T = \frac{-C_1(T - T_0)}{C_2 + (T - T_0)} \quad (4)$$

176 where C_1 and C_2 are model coefficients and T_0 is the reference temperature.

177 By fitting sigmoidal function and dynamic moduli data, the master curves constructed at
178 15°C reference temperature for all three mixtures are shown in Figure 5. Utilizing a nonlinear
179 minimization algorithm, the coefficients of sigmoidal function were computed and presented
180 in Table 3. Based on constructed master curves, AC moduli are determined at specified
181 frequencies and temperatures. Figure 6 shows the dynamic moduli determined at various
182 temperatures and a frequency of 5 Hz. In recent years, however, there was a controversial issue
183 in determination of frequency in asphalt pavements (ARA 2004; Al-Qadi et al. 2008).

184 **3.4. Determination of Loading Frequency in Pavements**

185 The applied load at a given point in the pavement causes a stress pulse at that point. The
186 rate of loading or the loading frequency depends on the duration of the stress pulse. The
187 following equation in MEPDG is utilized to determine the pulse duration:

188 $$t = \frac{L_{eff}}{17.6 v_s} \quad (5)$$

189 where *t* is the pulse duration (s); L_{eff} is the effective length (m); v_s is the vehicle speed (m/s).
190 The loading frequency is then determined as the reciprocal of *t.* The effective length, L_{eff} , is
191 the length that defines the extent of the stress pulse at the given depth within the pavement, as
192 schematically illustrated in Figure 7. The figure shows the stress distribution within various
193 layers caused by an axle load applied on top of the pavement. The sloped lines in the figure
194 represent the distribution of stress with depth. The spread or the steepness of the stress

distribution lines in a layer depends on material stiffness of the layer. A stiffer layer tends to distribute the stress over a wider area compared to a less stiff layer. To determine L_{eff}, the Odemark's method of equivalent thickness is adopted in the MEPDG to transform the pavement layers above the subgrade into one layer. The stress distribution lines in the transformed pavement are at 45 degrees, and thus the effective length at any depth can be determined. Details about the determination of L_{eff} are documented elsewhere (ARA 2004).

Furthermore, the AC layers are divided into different sublayers and the loading frequency of each sublayer is determined according to the procedure mentioned previously. Table 4 illustrates the dynamic moduli and loading frequencies computed at various temperatures for the thick and thin AC layers under dual tires loading. Using the layers moduli in LET, the pavements responses are computed.

3.5. Analysis of Non-Uniform Aging Gradient

In order to take into consideration non-uniform aging effect within AC layer depth in the mechanistic analysis, modulus gradient is considered as the crucial factor and calculated at various depths according to the Equations (6) and (7) (Ling et al. 2017a; Ling et al. 2019a):

$$E(z) = E_d + (E_0 - E_d)\left(\frac{d-z}{d}\right)^n \quad (6)$$

$$K = \frac{E_0}{E_d} \quad (7)$$

where *E(z)* is the dynamic modulus (MPa) of AC layer at depth *z*; E_d and E_0 are the dynamic moduli (MPa) at the bottom and top of asphalt layer, respectively; *d* is the AC thickness (cm); The *n* and *k* are the parameters of the model which presents the shape of the stiffness gradient. A stiffer surface modulus due to the effects of aging gradient produces a larger value of k. As

mentioned before, non-uniform aging gradient occurs at the top 4-5 cm pavement surface. Therefore, in this study modulus gradient is only considered non-uniform within SMA13 depths at different aging times. Analyses are conducted by dividing SMA13 layer into 1-cm-thick sublayers and calculating the corresponding modulus at each depth according to the aforementioned equations. Figures 8(*a* and *b*) depict the modulus gradients in the aged asphalt layer with an arbitrary surface modulus 2000 MPa.

3.6. Analysis of Non-Uniform Temperature Gradient

It should be noticed that the temperature is not uniform within the pavement depth (Roque et al. 2017; Archilla 2015; Raju et al. 2008). Consequently, in this study, temperature profile within the AC layer is assumed by presenting a rate of linear temperature differential of 1ºC/cm based on previous researches (Wang 2011; Sangpetngam et al. 2004). The temperature at pavement surface is considered as analysis temperature. However, temperature variations within the AC layer at low and high temperatures are considered as the negative and positive temperature gradients, respectively. By dividing the asphalt layer to several sublayers with equal thicknesses, the modulus at the middle of each sublayer is determined according to the corresponding temperature. For instance, Figure 9 illustrates the temperature gradients in a thick AC layer.

To investigate influence of the aforementioned parameters on TDC, the horizontal strains are computed at different temperatures, aging levels and vehicle speeds at the bottom and top of thick and thin asphalt layers. The circular uniform dual tires loading with a pressure of 0.7 MPa and a diameter of 20 cm is considered in the analyses, whereas the center-to-center distance of the dual tires is 30 cm.

4. Results and discussions

The horizontal strains at the bottom and top of thick and thin asphalt layers have been calculated at different transverse positions, ranging from the center of dual tires to a distance of 55cm. Significant analyses have been performed at three AC temperatures (5, 25 and 50°C), six vehicle speeds (8, 24, 48, 72, 96 and 120 km/h) and three aging gradient levels with the surface moduli of 500, 2000 and 8000 MPa for the pavements with CTB and GB.

4.1 Effect of temperature gradient in pavements with CTB

To identify the critical tensile strain at AC temperature of 5°C, the horizontal strain profiles at the top and bottom of thick and thin AC layers in low vehicle speed (8 km/h) are plotted in Figures 10(*a* and *b*), respectively. In the figures, ε_y indicates longitudinal (traffic direction) strains while ε_x represents transverse strains. In this paper, the positive and negative values represent the tensile and compressive strains, respectively. Because of symmetric boundary condition at dual tires center, the horizontal strains are only shown in the figures from the center of dual tires to a transverse distance of 55 cm.

It can be observed that in thick and thin asphalt layers, maximum tensile strains occur at the pavement surface and in transverse direction. The location of critical tensile strain is in the proximity of tire edge, which is in good agreement with the location of top-down fatigue cracking observed in the field studies (Matsuno and Nishizawa, 1992; Niderquell et al, 2000).

The horizontal strain profiles at temperature of 50°C in asphalt layers with different thicknesses are presented in Figures 11(*a* and *b*). It is seen that the maximum transverse strains at the top of thick and thin AC layers are 635.1 and 516.6 microstrains, respectively, while the horizontal strains values at the bottom of both AC layers are negative. This finding indicates

that TDC distress is severe at high temperature in pavements with CTB.

To explore the influence of temperature variations in pavements with CTB, the critical horizontal strains calculated at medium and high temperatures are compared with those at 5°C in Table 5. It is observed that in thick pavement with low speed (8km/h), the maximum transverse strain at the surface increases 5.7 and 38.3 times, while the longitudinal strain at the bottom decreases 1.8 and 3.4 times at 25°C and 50°C, respectively. Based on the results, longitudinal strain at the bottom and transverse strain at the top of asphalt layers are critical horizontal strains at pavement structures.

According to the strain profiles, the proximity of tire edge is a critical location of crack initiation, once the maximum tensile strain is at the surface. The results illustrate that the large value of surface tensile strain would be the main reason for TDC. It is noticed that in MEPDG, the points are exactly investigated at the tire edges which may lead to the smaller strain magnitudes and inaccurate estimation of critical response. For instance, in Figures 10(*a* and *b*), the critical transverse strains at a very close distance to the tire edge in thick and thin AC layers are 16.6 and 4.8 microstrains, respectively, and in tension, whereas those exactly at the tire edge are 4.53 and 17.2 microstrains and in compression. This finding indicates that the MEPDG may not be capable of determining critical tensile strain at the pavement surface correctly.

4.2 Effect of temperature gradient in pavements with GB

To explore the likelihood of TDC in pavements with GB at different AC temperatures, numerous analyses have been conducted to compute the critical horizontal strains in AC layers. The strain profiles in thick and thin AC layers at a temperature of 50°C are presented in Figures 12(*a* and *b*), respectively.

From the figures, it is observed that utilizing GB layer in pavements, increase horizontal strains at the bottom and decrease those at the top of thick and thin AC layers. However, the peak value of longitudinal strain at the bottom of thick AC layer is 318.1 microstrains, TDC is dominant type of distress in thick pavements with GB at 50°C. Due to the similar values of the critical strains at the top and bottom of thin asphalt layer, cracking is likely to initiate at any of the corresponding locations. The critical horizontal strain responses in pavements with GB at various AC temperatures and thicknesses are illustrated in Table 5. Compared to maximum longitudinal strain at the bottom of thick AC layer, maximum transverse strain value at the top is small (2.4 and 12.9 microstrains at 5°C and 25°C, respectively), which indicates its insignificant contribution to TDC initiation.

According to the strain response profiles at the surface, transverse strain is more critical than longitudinal strain, while at the bottom of asphalt layer tensile strain in longitudinal direction is more significant than that in transverse direction. Hence, only these two critical responses are considered in further analyses.

4.3 Effect of vehicle speed in pavements with CTB

To Investigate vehicle speeds impact on TDC, horizontal strains at the top and bottom of AC layers were calculated at vehicle speeds of 8, 24, 48, 72, 96 and 120 km/h. Variations of maximum horizontal strains with vehicle speeds in thick and thin AC layers are illustrated in Figures 13(*a* and *b*), respectively, at low temperature in pavements with CTB. According to the figures, the strain responses at the top and bottom of AC layers display the reverse trends. In both AC layers, reducing vehicle speed from 120 km/h to 8 km/h leads to the increase of transverse strain at the top of thick AC layer more than 2 times and decrease of longitudinal

304 strain at the bottom of thin AC layer more than 2.9 times.

305 As seen in Figure 13*a*, TDC is the critical type of distress in thick AC layer at all speeds
306 analyzed. However, at vehicle speeds higher than 96 km/h, longitudinal strain value at the
307 bottom is 8.1 microstrains which is almost similar to transverse strain at the top of asphalt layer.
308 This observation indicates that cracking may initiate at the same time at top and bottom of thick
309 asphalt layer or first at either of those locations. On the contrary, bottom-up cracking is
310 dominant in the thin AC layer at medium and high speeds. Only if the vehicle moves less than
311 10 km/h, transverse strains at surface may become critical. The critical horizontal strains
312 calculated at different vehicle speeds in thick and thin AC layers is presented in Table 6.

313 The results at medium and high temperatures show that longitudinal strains at the bottom
314 are compressive or very small (less than 2 microstrains), while the speed variations influence
315 on the transverse strains at pavement surface is tremendous. It is also seen from the table that
316 maximum transverse strains increase exponentially as the speeds decrease. This is expected
317 because loading frequency reduction is equivalent to temperature increase, based on time-
318 temperature superposition principle.

319 **4.4 Effect of vehicle speed in pavements with GB**

320 As demonstrated before, pavements with GB are prone to TDC only at high temperature.
321 To find critical horizontal strains in pavements with GB at various speeds, the response profiles
322 in thick and thin AC layers are plotted in Figures 14(*a* and *b*), respectively. It is seen that by
323 decreasing the vehicle speeds, critical strains increase at the top and bottom of AC layers.
324 Within ranges of 24-120km/h, however, rate of increase in transverse strain is from 92.95 to
325 257.4 microstrains and faster than longitudinal strain at the bottom AC layers, bottom-up

cracking is predominant type of distress. Instead, at vehicle speed of 8 km/h, TDC becomes pronounced in pavements with GB. The critical horizontal strains at different speeds and temperatures in thick and thin AC layers is illustrated in Table 7.

The results in the table reveal that lower speeds result in higher strains at the bottom and top of AC layers at 5 and 50°C, respectively. Once the speed decreases from 24 to 8 km/h, 78.6 percent increase in transverse strain is observed at 50°C in thick AC layer. In fact, pavements with GB are not only subjected to bottom-up cracking, but also TDC becomes a serious concern when the vehicle is moving slowly in pavements with various thicknesses.

4.5. Effect of non-uniform aging gradient in pavements

In order to investigate the non-uniform aging gradient effect on TDC in the pavements with CTB and GB, horizontal tensile strains are calculated at the top and bottom of aged AC layers with different thicknesses. By considering surface moduli of 500, 2000 and 8000 MPa which simulate the long-term aging at various times, the transverse strains at the top of SMA13 in thick and thin AC layers were obtained as the critical horizontal strain for different n and k values. Due to the similar trends obtained from the pavements with CTB and GB, transverse strain profiles at the top of SMA13 in thick pavement with CTB is depicted in Figures 15(*a* and *b*).

As shown in the figures, maximum transverse strain at the pavement surface is around 400 microstrains, when the surface modulus is 500 MPa. By increasing surface modulus to 8000 MPa, pavement surface becomes brittles and maximum transverse strain declines 8 times in its magnitude. However, this finding specifies that the hardening of pavement surface decreases strength and corresponding strain, TDC is the dominant type of cracking by considering the

348 stiffness gradient within AC depth. Since the horizontal strains at the bottom of AC layer are in
349 compression, the results are not shown herein.

350 Because of the significant effect of aging on TDC, it is important to investigate the critical
351 location of TDC at the surface at various aging times and different AC thicknesses. To do this,
352 transverse strains at the top of pavement with different surface moduli are calculated at 24
353 transverse locations ranging from the center of dual tires to a distance of 55 cm. The analyses
354 are conducted for n and k values equal to 3 and 2, respectively. The transverse strain profiles
355 obtained from the thick pavement with CTB and thin pavement with GB are illustrated in
356 Figures 16(*a* and *b*), respectively.

357 The figures show that at low surface modulus, critical location of TDC is exactly outside
358 of the tire edge. By increasing the surface modulus, the critical location of TDC occurs far from
359 the tire edge so that at surface modulus of 8000 MPa, center of dual tires becomes the critical
360 location of TDC. Therefore, critical location of TDC is highly dependent upon the age-
361 hardening level at the surface in both thick and thin AC layers.

362 Overview of the results show that TDC in pavements with CTB is the predominant type
363 of distress at various temperatures, while in pavements with GB, it is likely to take place only
364 at high temperture. Besides, the chance of TDC initiation increases with decreasing the vehicle
365 speed and increasing the temperature in both thick and thin AC layers, while the age hardening
366 level changes the critical location of TDC at the surface. Since the failure mechanisms of top-
367 down and bottom-up cracking have just been explored in this study, the conclusions have been
368 drawn based on comparison of these two cases in the thick and thin pavements with CTB and
369 GB.

5. Conclusions

Accurate determination of pavement responses at the surface plays an important role in the structure design and prediction of TDC. In this study, the effects of speed (loading frequency), temperature and non-uniform aging gradients on TDC are investigated by calculating maximum horizontal strains at the thick and thin asphalt layer surface. Analyses are conducted for the pavements with CTB and GB.

This new analysis approach uses the Lucas algorithm and the integration, summation and then extrapolation method to compute the horizontal strains precisely. The results obtained are summarized as follows:

- The critical location of the tensile strain is in the proximity of tire edges, which indicates the results agree well with the typical pattern of the TDC observed in the field. The locations adopted in the MEPDG are inadequate and thus the maximum tensile strain at the surface may not be identified.
- Pavements with CTB are vulnerable to TDC at different temperatures and AC thicknesses. Because of strong support from the base layer, horizontal strains at the bottom of AC layers are very small or in compression.
- Utilizing GB in thick and thin pavements causes the bottom-up cracking to be the dominant type of fatigue failure at low and medium temperatures, while at high temperature cracking is likely to initiate simultaneously at the top and bottom or AC layers with different thicknesses.
- Variations of surface modulus due to the aging cause the critical location of TDC to vary noticeably from outside of the tire edge to the center of dual tires. This finding is

consistent with the characteristic of the TDC observed in the field. In addition, increasing aging time leads to the reduction in tensile strength of the thick and thin AC layers and horizontal tensile strains at surface.

- Compared to the longitudinal strain at the bottom of AC layer, transverse strain magnitude at the surface is more induced at lower speeds which result in TDC.
- At low temperature and higher speeds, the magnitudes of maximum longitudinal strain at the bottom and transverse strain at the surface of thick AC layer are almost the same and occur just outside of the tire edge. Therefore, the failure may occur at the same time at the bottom and top of asphalt layers in pavements with CTB.
- For the pavements with GB, the influence of speed reductions on longitudinal strain in thin AC layer is greater than that in the thick AC layer. But, once the vehicle moves slowly at high temperature, TDC becomes a serious concern.

However, the results of this research provide beneficial insight to analysis and design of asphalt pavements from a mechanistic point of view, considering more pavement structures is recommended in the future studies.

Acknowledgments

This research was sponsored by National Natural Science Foundation of China [grant number 51678114], Inner Mongolia Transportation Research Project [grant number NJ-2014-21], Liaoning Transportation Research Project [grant number 201309] and Shanxi Transportation Research Project [grant number 2015-1-22]. The authors gratefully

413 acknowledge their financial support.

414

415 **References**

416 Al-Qadi, I. L., Xie, W., & Elseifi, M. A. (2008). Frequency determination from vehicular
417 loading time pulse to predict appropriate complex modulus in MEPDG. Asphalt Paving
418 Technology-Proceedings, 77, 739.

419 Al-Rub, R. K. A., Darabi, M. K., Kim, S. M., Little, D. N., & Glover, C. J. (2013). Mechanistic-
420 based constitutive modeling of oxidative aging in aging-susceptible materials and its effect
421 on the damage potential of asphalt concrete. Construction and Building Materials, 41, 439-
422 454.

423 American Association of State Highway and Transportation officials (AASHTO), (2007).
424 "Standard method of test for determining dynamic modulus of hot-mix asphalt (HMA)."
425 AASHTO TP 62-07, Washington, DC.

426 Applied Research Associates. (2004). Guide for mechanistic-empirical design of new and
427 rehabilitated pavement structures. Final Report, National Cooperative Highway Research
428 Program (NCHRP) Project 1-37A. Albuquerque, NM: National Research Council.

429 Archilla, A. R. (2015). Top-Down fatigue Cracking in High-Temperature Environments.
430 Transportation Research Record: Journal of the Transportation Research Board, (2507),
431 128-137.

432 Asphalt Institute. (1991). Asphalt pavement thickness design for highways and streets (MS-1).

433 Lexington, Kentucky: Author.

434 Burmister, D. M. (1943). The theory of stress and displacements in layered systems and
435 applications to the design of airport runways. Highway Research Board, Proceedings of
436 23rd Annual Meeting, 23, 126–144.

437 Chatti, K., Kim, H., Yun, K., Mahoney, J., & Monismith, C. (1996). Field investigation into
438 effects of vehicle speed and tire pressure on asphalt concrete pavement
439 strains. Transportation Research Record: Journal of the Transportation Research Board,
440 (1539), 66-71.

441 Chun, S., Kim, K., Greene, J., & Choubane, B. (2018). Evaluation of top-down cracking
442 potential for asphalt pavements with 4.75 mm nominal maximum aggregate size mixture
443 layer using full-scale field tests and finite element analysis. Road Materials and Pavement
444 Design, 19(5), 1089-1101.

445 Dinegdae, Y. H., & Birgisson, B. (2018). Effects of truck traffic on top-down fatigue cracking
446 performance of flexible pavements using a new mechanics-based analysis framework.
447 Road Materials and Pavement Design, 19(1), 182-200.

448 Dai, S. T., Van Deusen, D., Beer, M., Rettner, D., & Cochran, G. (1997). Investigation of
449 flexible pavement response to truck speed and FWD load through instrumented pavements.
450 In 8th International Conference on Asphalt Pavements Federal Highway Administration.

451 Davis, P. J., & Rabinowitz, P. (1988). Methods of numerical integration. Orlando, FL: Academic
452 Press.

453 Evans, G. (1993). Practical numerical integration. Delft, Netherland: John Wiley & Sons.

454 Ferry, J.D. (1980). Viscoelastic properties of polymers, 3rd edition. John Willey & Sons., New
455 York.

456 Gu, F., Luo, X., West, R. C., Taylor, A. J., & Moore, N. D. (2018). Energy-based crack initiation
457 model for load-related top-down cracking in asphalt pavement. Construction and Building
458 Materials, 159, 587-597.

459 Huang, Y. (2003). Pavement analysis and design. Englewood Cliffs, New Jersey: Prentice Hall.

460 Kim, J., Roque, R., and Byron, T. (2009). Viscoelastic Analysis of Flexible Pavements and Its
461 Effects on Top-Down Cracking. Journal of Materials in Civil Engineering, ASCE, 21(7):
462 324-332.

463 Ling, M., Luo, X., Hu, S., Gu, F., & Lytton, R. L. (2017a). Numerical modeling and artificial
464 neural network for predicting J-integral of top-down cracking in asphalt
465 pavement. Transportation Research Record: Journal of the Transportation Research
466 Board, (2631), 83-95.

467 Ling, M., Luo, X., Gu, F., & Lytton, R. L. (2017b). Time-temperature-aging-depth shift
468 functions for dynamic modulus master curves of asphalt mixtures. Construction and
469 Building Materials, 157, 943-951.

470 Ling, M., Luo, X., Chen, Y., Gu, F., & Lytton, R. L. (2018). Mechanistic-empirical models for
471 top-down cracking initiation of asphalt pavements. International Journal of Pavement

472 Engineering, 1-10.

473 Ling, M., Chen, Y., Hu, S., Luo, X., & Lytton, R. L. (2019a). Enhanced model for thermally
474 induced transverse cracking of asphalt pavements. Construction and Building
475 Materials, 206, 130-139.

476 Ling, M., Luo, X., Chen, Y., Hu, S., & Lytton, R. L. (2019b). A calibrated mechanics-based
477 model for top-down cracking of asphalt pavements. Construction and Building
478 Materials, 208, 102-112.

479 Lourens, J. P. (1992). Nonlinear dynamic analysis and design of road pavements. Department
480 of Transport, Chief Directorate, Roads.

481 Lucas, S. K., & Stone, H. A. (1995). Evaluating infinite integrals involving Bessel functions of
482 arbitrary order. Journal of Computational and Applied Mathematics, 64(3), 217-231.

483 Matsuno, S., and Nishizawa. T. (1992). “Mechanism of Longitudinal Surface Cracking in
484 Asphalt Pavement”, Proc. of 7th International Conference on Asphalt Pavements, The
485 University of Nottingham, 277-291.

486 Mikhail, M., & Mamlouk, M. (1997). Effect of vehicle-pavement interaction on pavement
487 response. Transportation Research Record: Journal of the Transportation Research Board,
488 (1570), 78-88.

489 Mohammad, F. A., Collop, A. C., & Brown, S. F. (2005). Effects of surface cracking on
490 responses in flexible pavements. Proceedings of the Institution of Civil Engineers –

Transport, 158(2), 127–134.

Myers, L. A., Roque, R., & Ruth, B. E. (1998). Mechanisms of surface-initiated longitudinal wheel path cracks in high-type bituminous pavements. Journal of the Association of Asphalt Paving Technologists, 67.

Niederquell, M., Baladi, G., & Chatti, K. (2000). Rubblization of concrete pavements: Field investigation. Transportation Research Record: Journal of the Transportation Research Board, (1730), 150-160.

Perret, J., & Dumont, A. G. (2004). Strain and stress distributions in flexible pavements under moving loads. Road Materials and Pavement Design, 5(sup1), 203-225.

Qin, F., Yu, Y., & Rudolphi, T. (2010). Finite element modeling of viscoelastic stress analysis under moving loads. Int. J. Mech. Mater. Eng, 1(4), 226-233.

Rahman, A., Huang, H., Ai, C., Ding, H., Xin, C., & Lu, Y. (2019). Fatigue performance of interface bonding between asphalt pavement layers using four-point shear test set-up. International Journal of Fatigue, 121, 181-190.

Roque, R., Kim, J., & Byron, T. (2006). Evaluation of surface-initiated longitudinal wheel path cracking (Final Rep. for FDOT No. C5978 Contract). Gainesville: University of Florida.

Sarkar, A. (2016). Numerical comparison of flexible pavement dynamic response under different axles. International Journal of Pavement Engineering, 17(5), 377-387.

Shell International Petroleum Company. (1978). Shell pavement design manual. London:

510 Author.

511 Siddharthan, R. V., Krishnamenon, N., El-Mously, M., & Sebaaly, P. E. (2002). Validation of a
512 pavement response model using full-scale field tests. International Journal of Pavement
513 Engineering, 3(2), 85-93.

514 Sidi, A. (1988). A user-friendly extrapolation method for oscillatory infinite integrals.
515 Mathematics of Computation, 51(183), 249–249.

516 Svasdisant, T., Schorsch, M., Baladi, G., & Pinyosunun, S. (2002). Mechanistic analysis of top-
517 down cracks in asphalt pavements. Transportation Research Record: Journal of the
518 Transportation Research Board, (1809), 126-136.

519 Wambura, J. H., Maina, J., & Smith, H. R. (1999). Kenya bituminous materials
520 study. Transportation research record, 1681(1), 129-137.

521 Wang, H., Ozer, H., Al-Qadi, I. L., & Duarte, C. A. (2013). Analysis of near-surface cracking
522 under critical loading conditions using uncracked and cracked pavement models. Journal
523 of Transportation Engineering, 139(10), 992-1000.

524 Wu, S., Wen, H., Zhang, W., Shen, S., Mohammad, L. N., Faheem, A., & Muhunthan, B. (2019).
525 Field performance of top-down fatigue cracking for warm mix asphalt
526 pavements. International Journal of Pavement Engineering, 20(1), 33-43.

527 Zhao, Y., Zhou, C., Zeng, W., & Ni, Y. (2015). Accurate determination of near-surface responses
528 of asphalt pavements. Road Materials and Pavement Design, 16(1), 186–199.

Alae, M., Zhao, Y., Zarei, S., Fu, G., & Cao, D. (2018). Effects of layer interface conditions on top-down fatigue cracking of asphalt pavements. International Journal of Pavement Engineering, 1-9. DOI: 10.1080/10298436.2018.1461870.

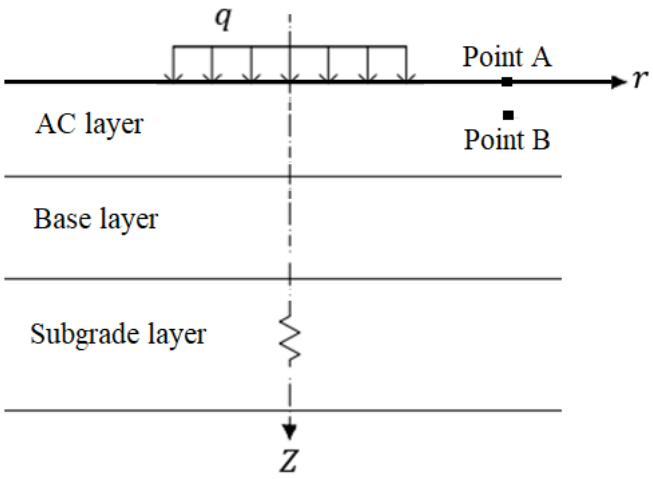

Figure 1. Geometry of the pavement structure with analysis points "A" and "B"

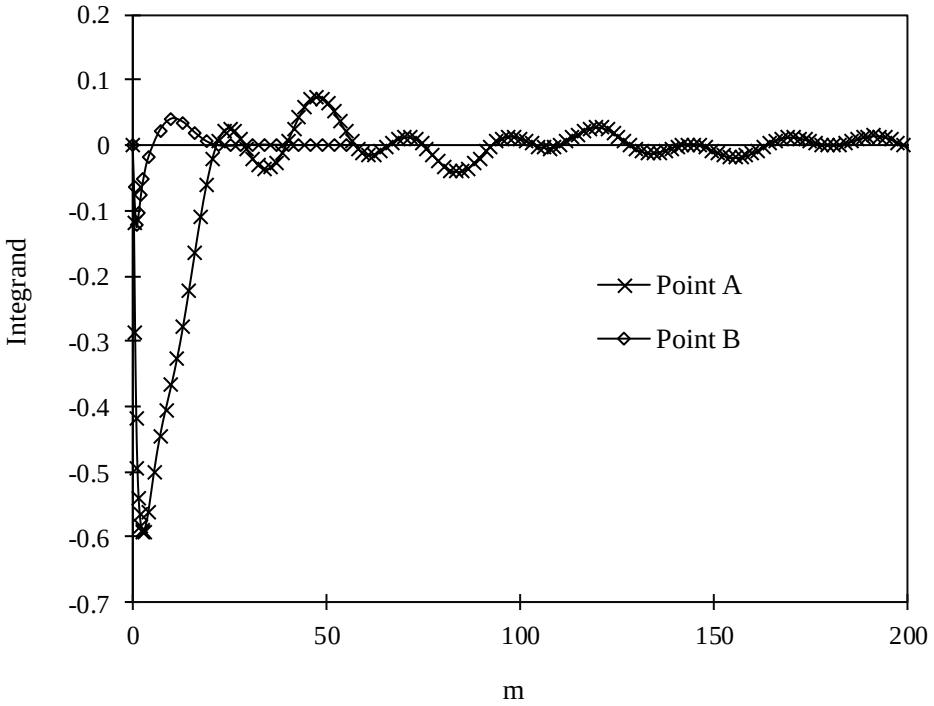

Figure 2. Integrand oscillation of the Burmister's solution

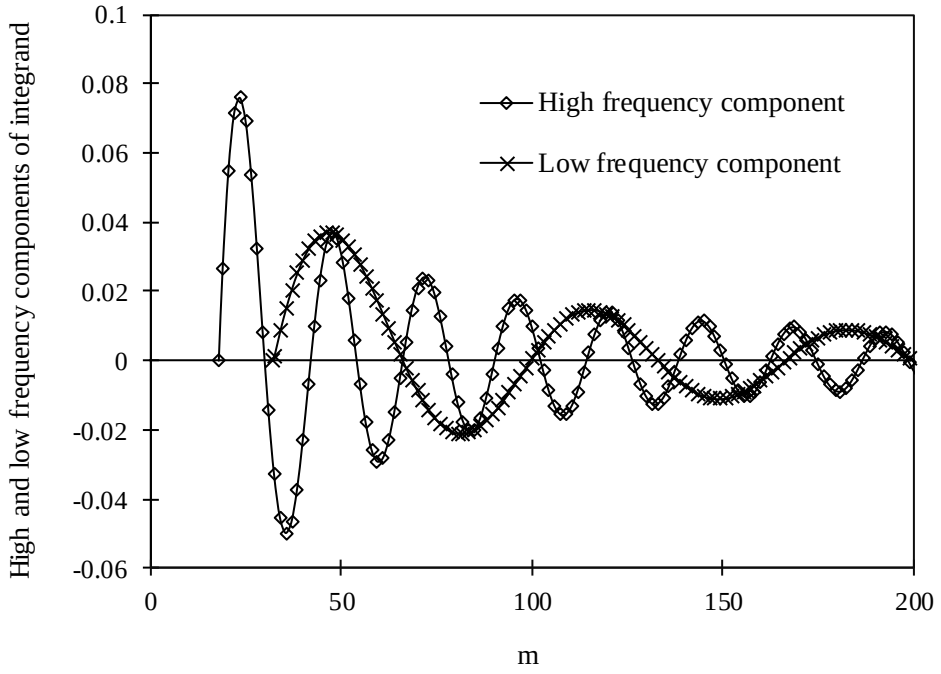

Figure 3. Illustration of low and high frequency components

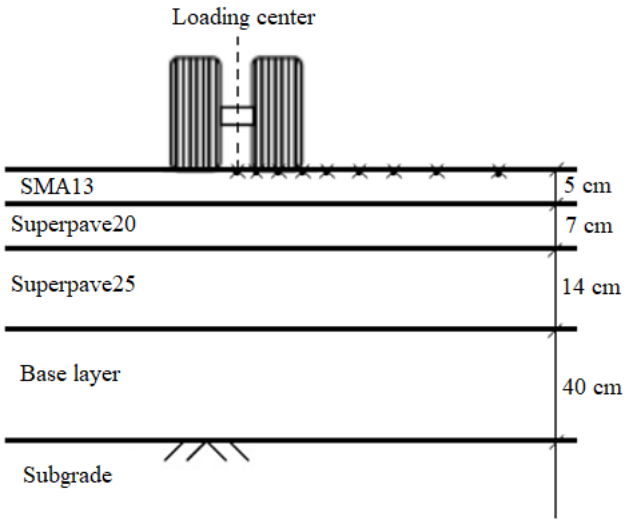

(a)

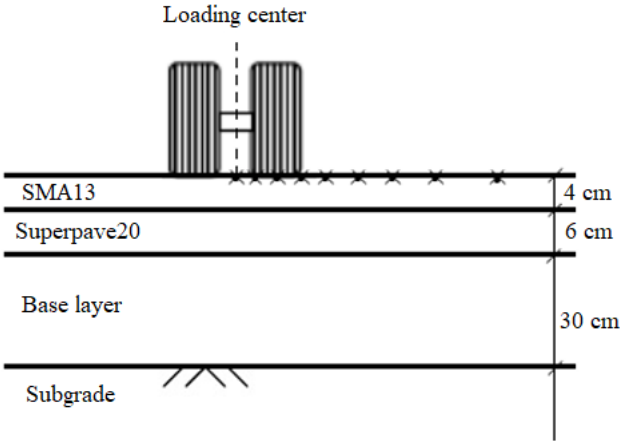

(b)

Figure 4. Schematic of dual tires loading and analysis locations in: (a) Thick pavement structure (b) Thin pavement structure.

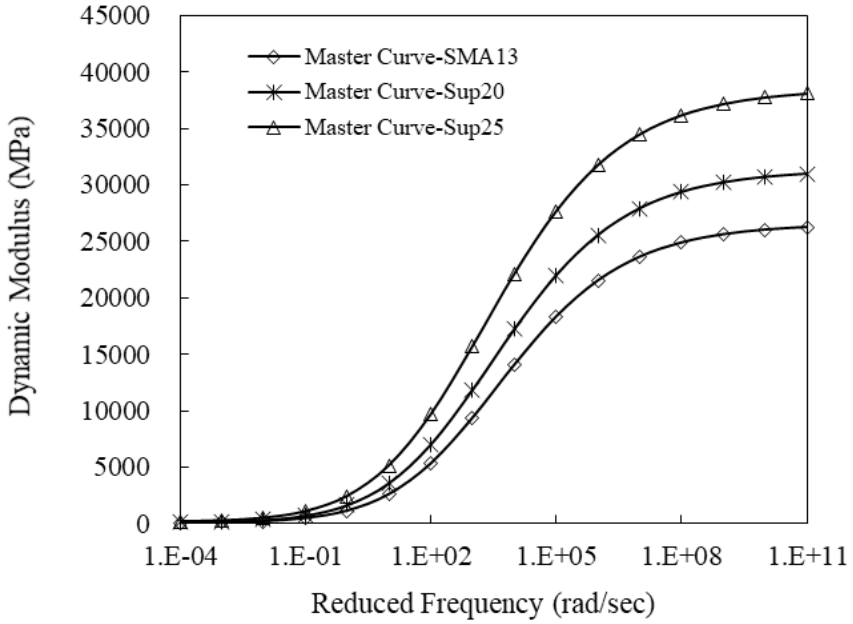

620

621 Figure 5. Dynamic moduli master curves constructed for three asphalt mixtures

622

623

624

625

626

627

628

629

630

631

632

633

634

635

636

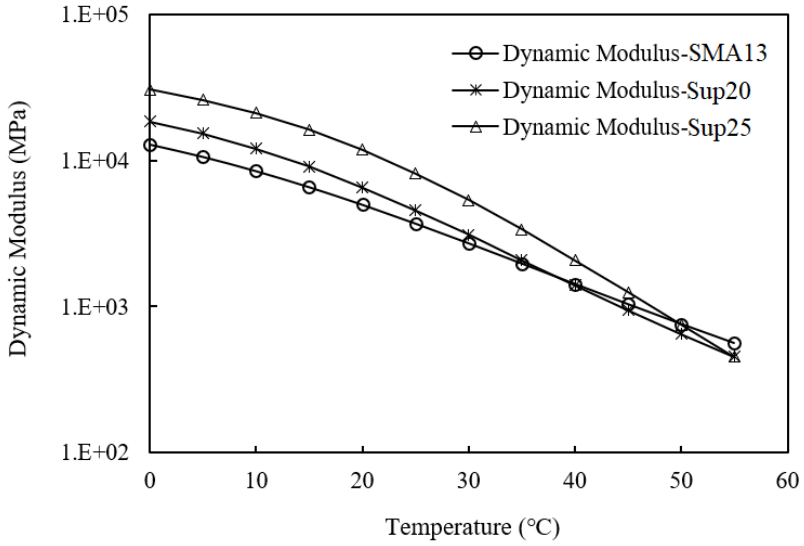

637

638 Figure 6. Dynamic moduli changes with temperature

639
640
641
642
643
644

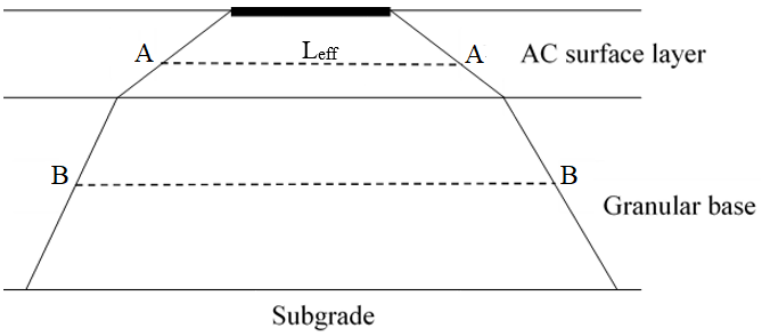

645

646 Figure 7. Illustration of the effective length

647
648
649
650
651
652
653
654
655
656
657
658

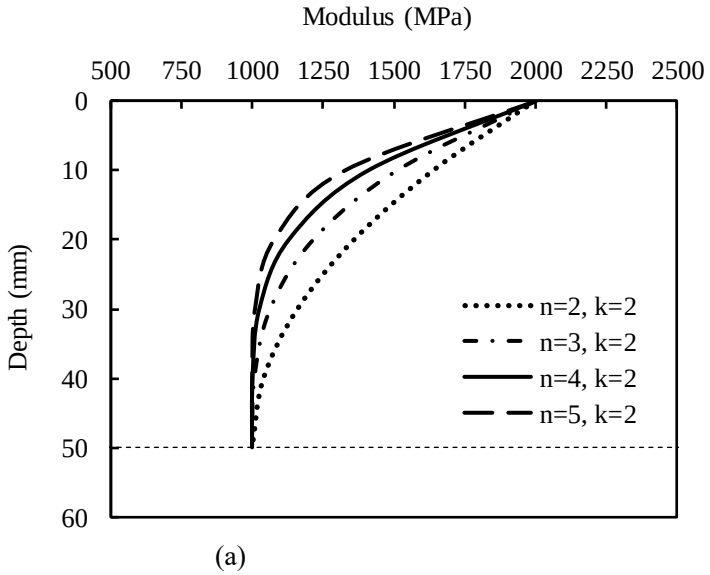

(a)

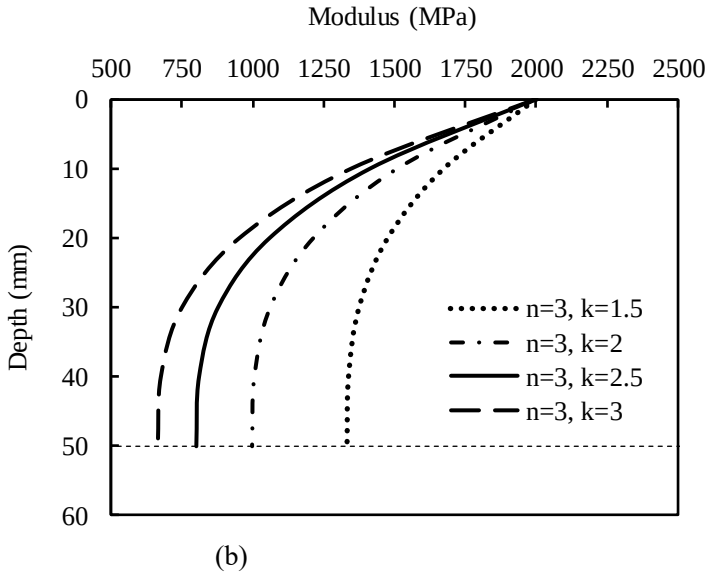

(b)

Figure 8. Non-uniform modulus gradient of aged SMA13 layer for various (a): *n* and (b): *k*

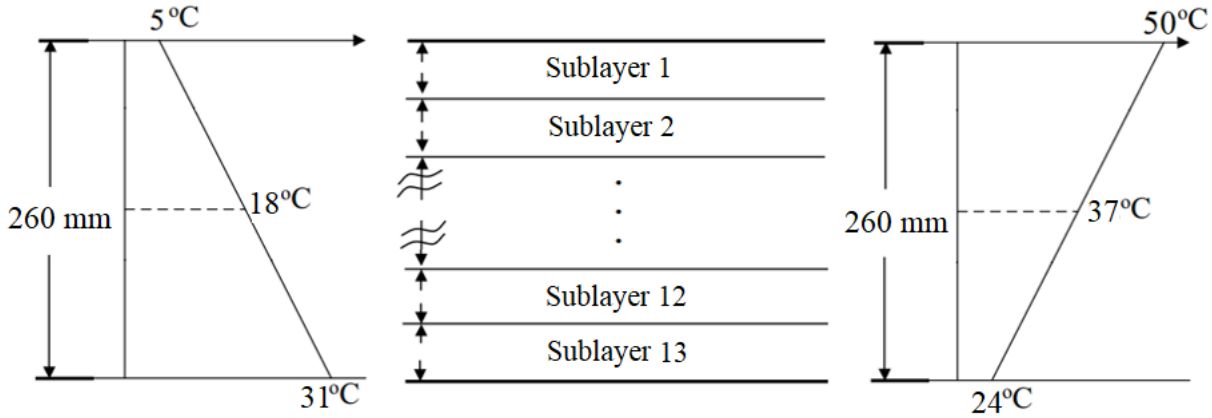

Figure 9. Illustration of negative and positive temperature gradients with various sublayers

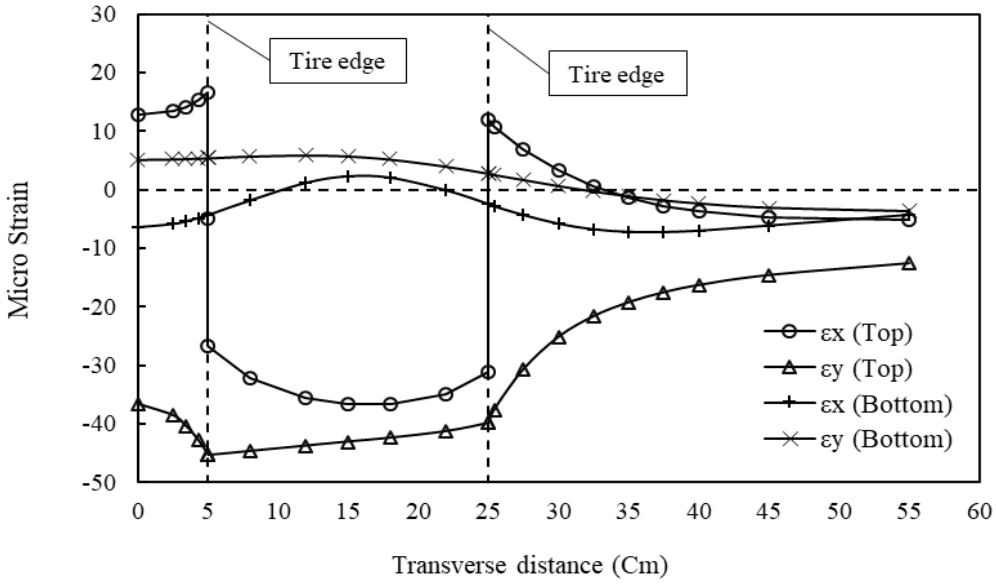

(a)

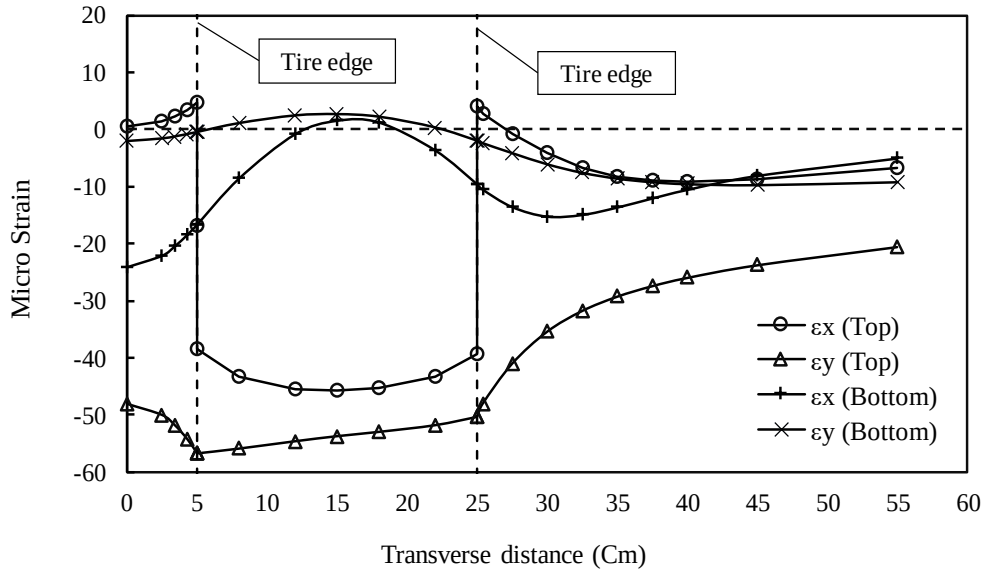

(b)

Figure 10. Critical locations of horizontal strains at low speed (5°C, CTB) in: (a) thick AC layer (b) thin AC layer

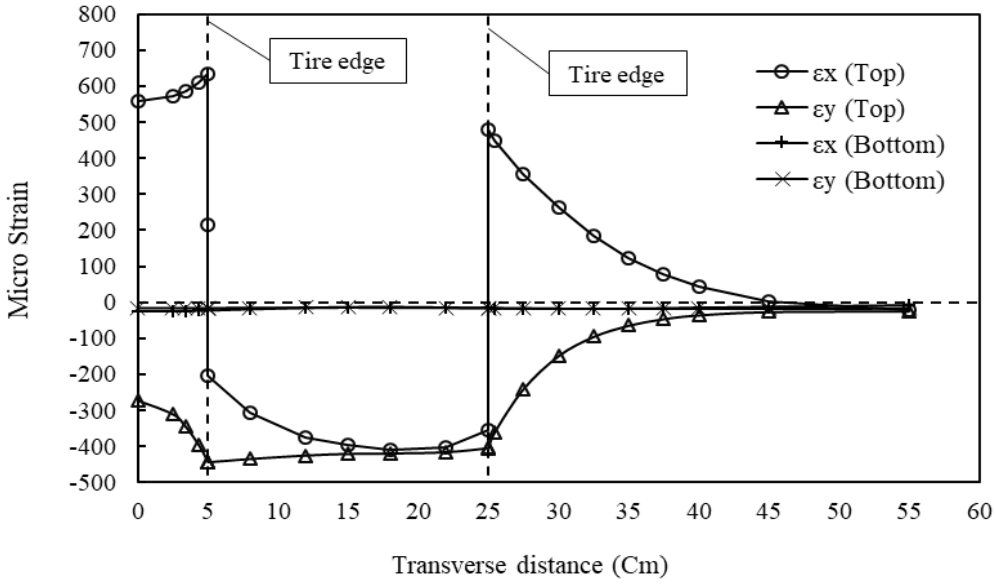

(a)

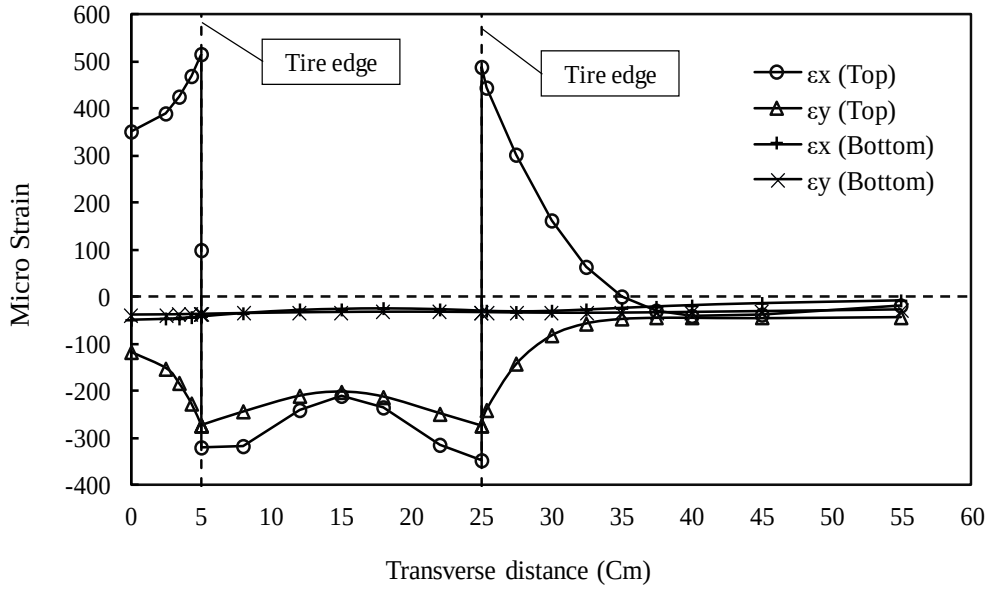

(b)

Figure 11. Critical locations of horizontal strains at low speed (50°C, CTB) in: (a) thick AC layer (b) thin AC layer

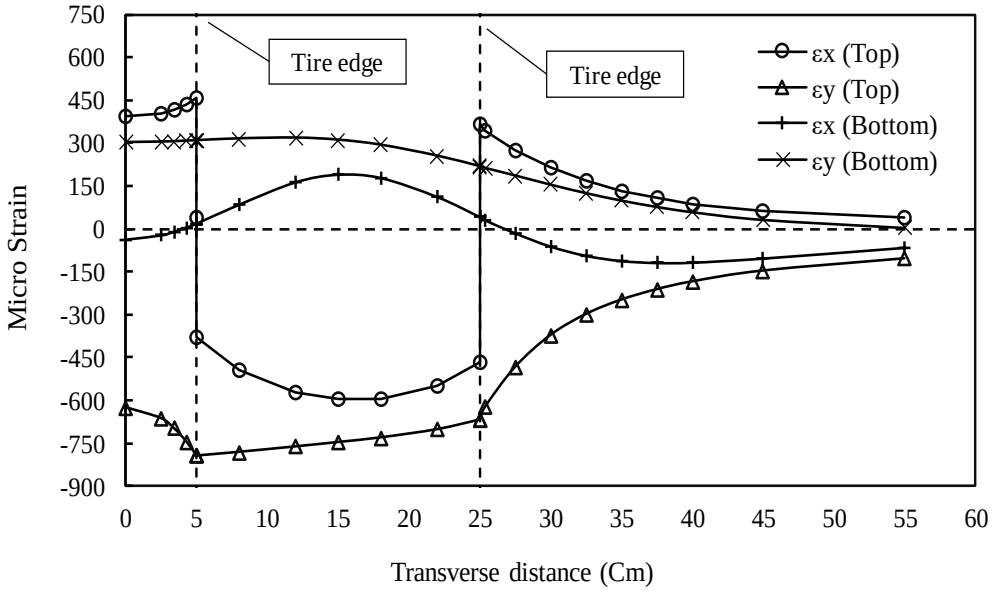

(a)

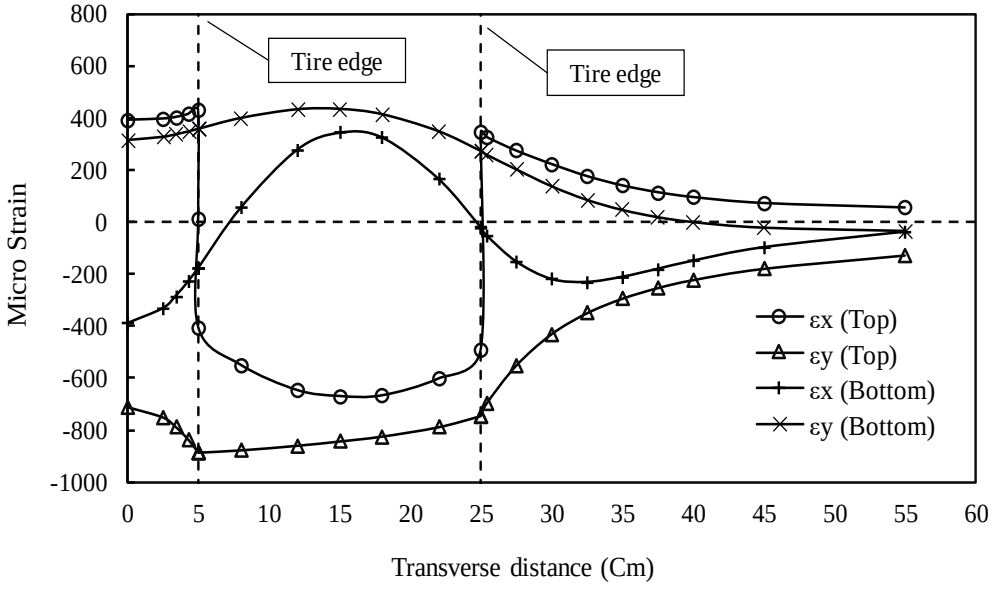

(b)

Figure 12. Critical locations of horizontal strains at low speed (50°C, GB) in: (a) thick AC layer (b) thin AC layer

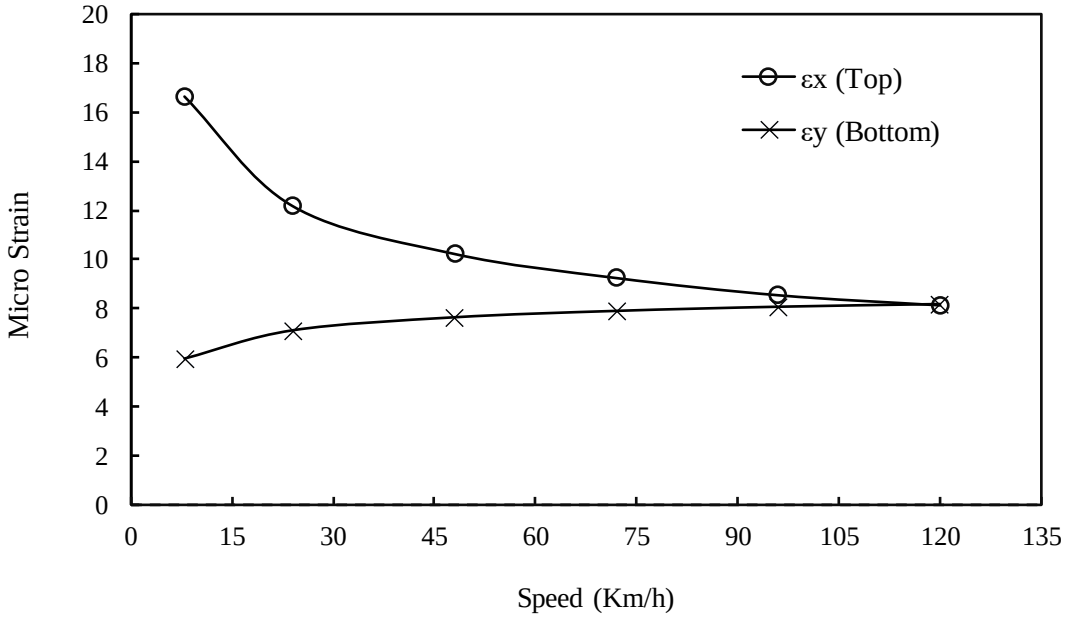

(a)

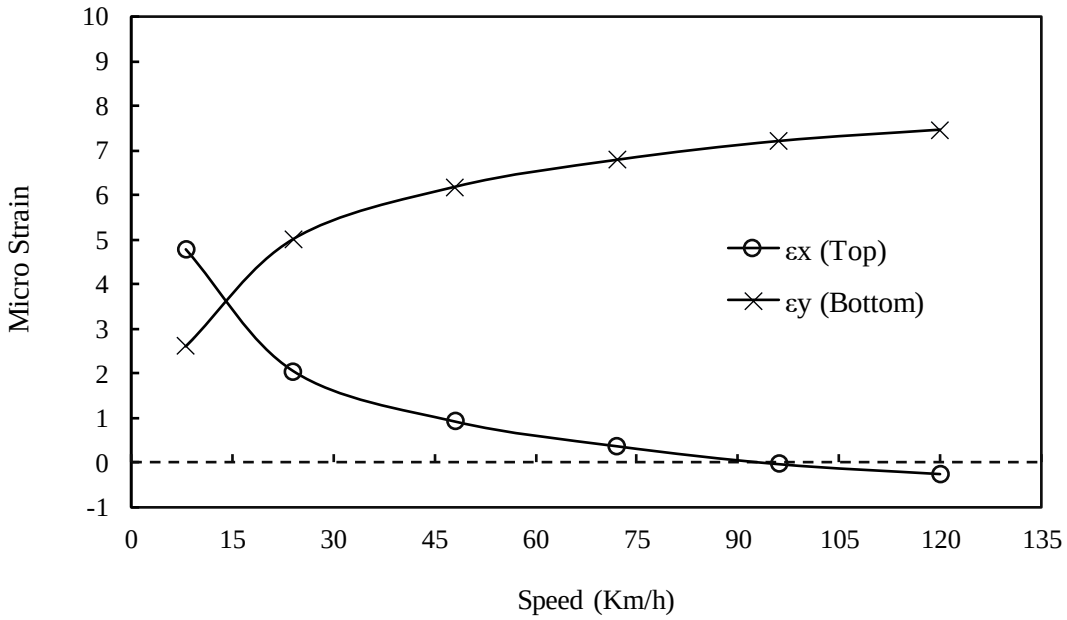

(b)

Figure 13. Variations of maximum horizontal strains with vehicle speeds (5°C, CTB) in: (a) thick AC layer (b) thin AC layer

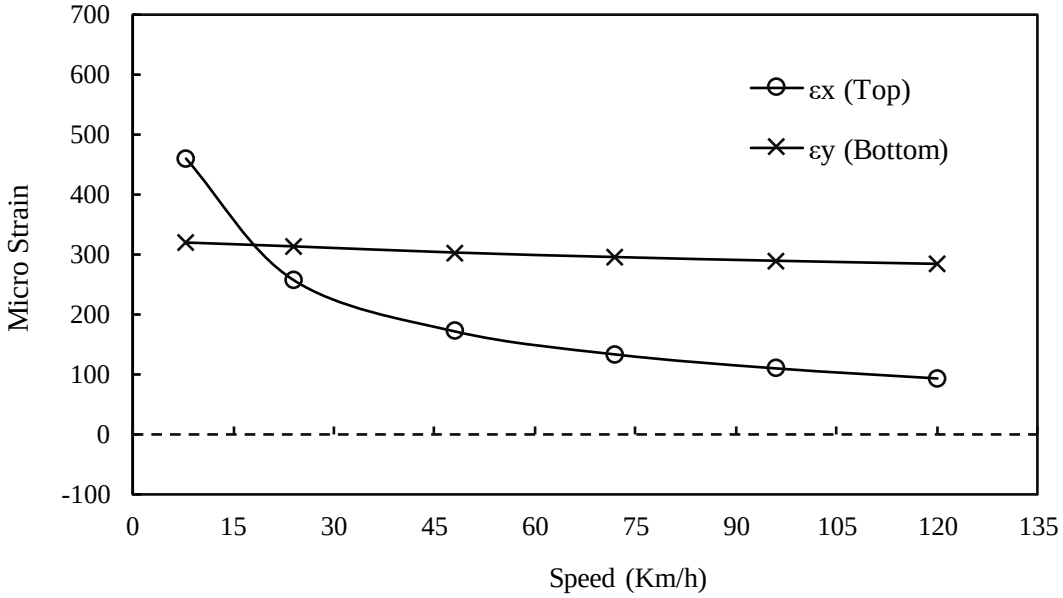

(a)

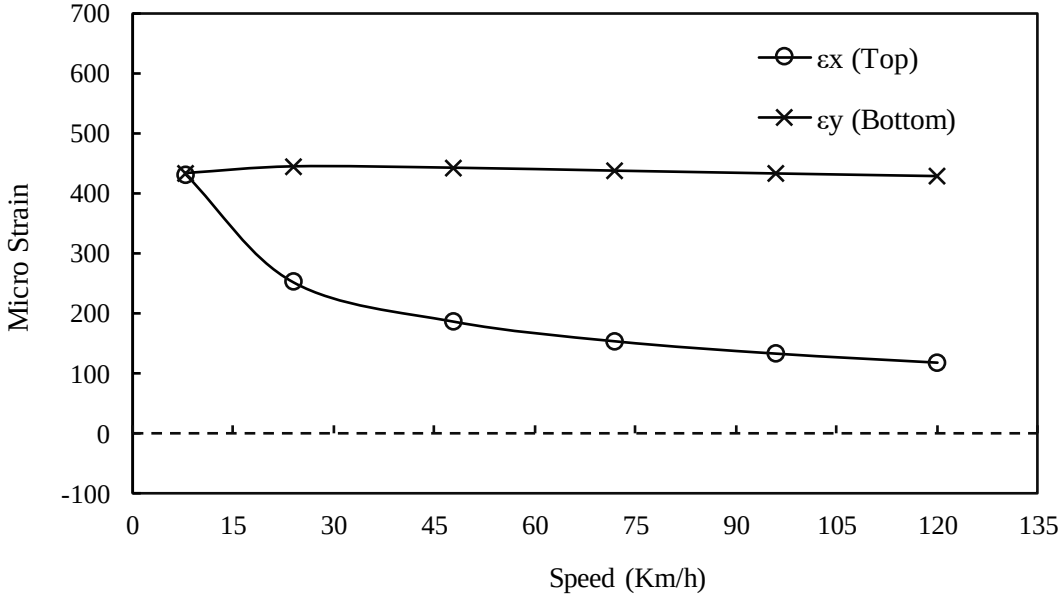

(b)

Figure 14. Variations of maximum horizontal strains with vehicle speeds (50°C, GB) in: (a) thick AC layer (b) thin AC layer

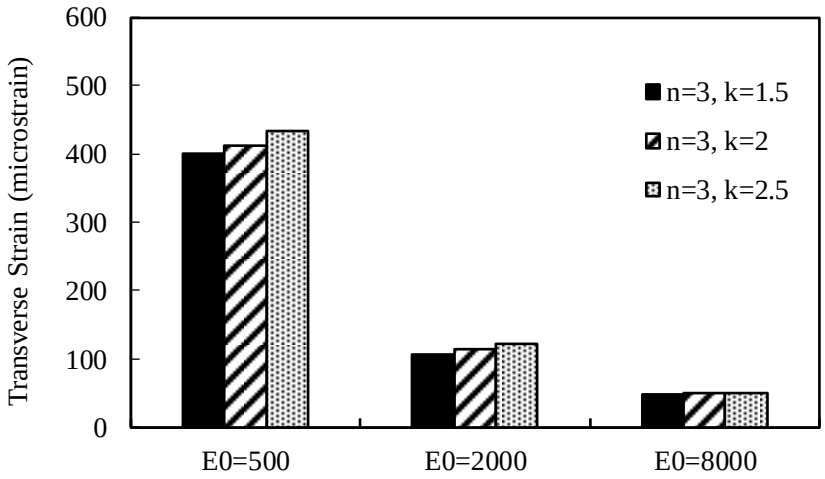

(a)

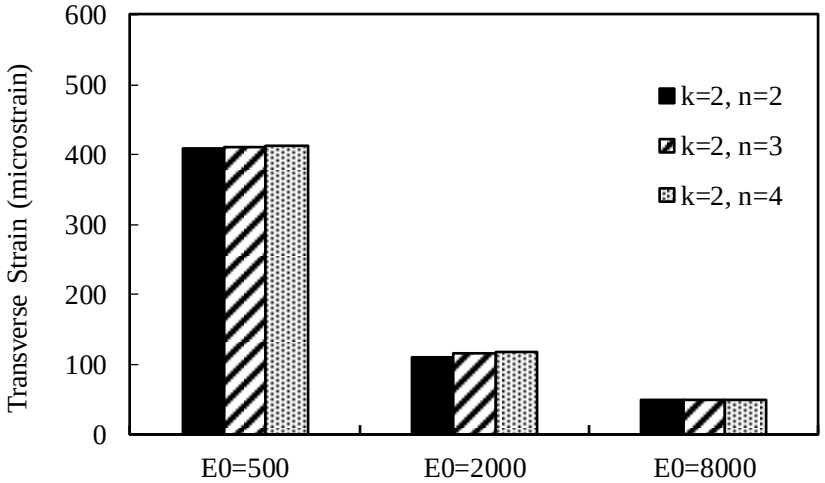

(b)

Figure 15. Maximum transverse strains at the top of aged AC layer with various surface moduli: (a) different *n*, (b) different *k*,

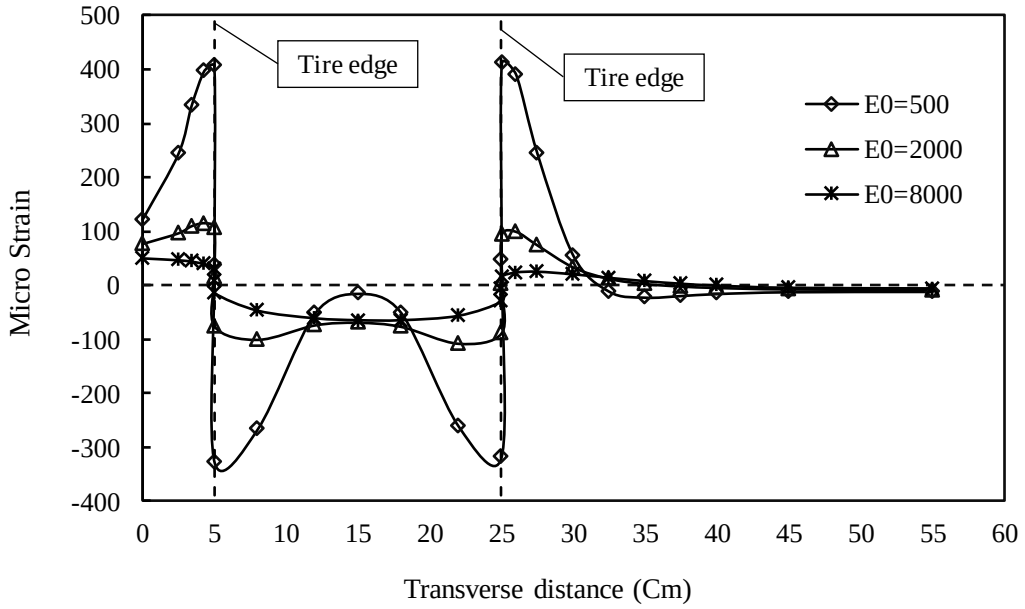

760

761 (a)

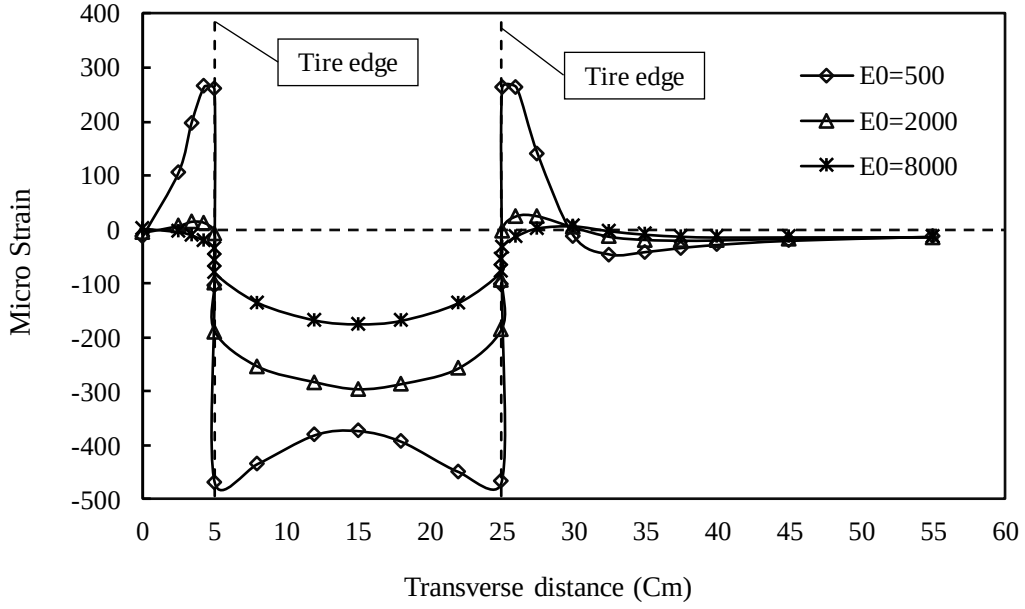

762

763 (b)

764 Figure 16. Variation of transverse strains with surface moduli at the top of aged AC layer in:

765 (a) thick pavement with CTB, (b) thin pavement with GB

766

767

768

769

770

771

772

773 Table 1. Pavement structure parameters used in analyses

Layer	Thickness (cm)	Modulus (mpa)	Poisson's ratio	TDC Depth (mm)	TDC Location
HMA	10, 20, 30	Using Prony series fitted parameters	0.3	4, 8, 24, 40, 56, 72, 88	C1, C2, C3, C4, C5, C6
Base	30	280 (GB) 7000 (CTB)	0.35 0.25	-	-
Subgrade	-	60	0.4	-	-

774

775

776

777

778

779

780

781

782

783

784

785

786

787

788

789

790

791

792

793

794

795

796

797

798 Table 2. Aggregate gradations for asphalt mixtures

Sieve size (mm)	Percentage passing (%)		
	Sup25 mixture	Sup20 mixture	SMA13 mixture
37.5	100	100	100
25	97	100	100
19	89	99	100
12.5	77	87	98
9.5	69	74	84
4.75	47	50	34
2.36	26	36	21
1.18	16	27	14
0.6	11	21	10
0.3	8	16	7
0.15	6	10	5
0.075	4.2	6.2	3.5

799

800

801

802

803

804

805

806

807

808

809

810

811

812

813

814

815

816

Table 3. Coefficients of MHN model

Mix Type	E_{∞}^{*} (mpa)	E_{0}^{*} (mpa)	α	β	ω_0	C_1	C_2
SMA13	26317	51.1	0.266	1.693	657.1	21.7	183.5
Sup20	32128	104.8	0.257	1.733	407.9	15.3	139.0
Sup25	38558	134.9	0.249	1.804	212.3	11.6	105.4

Table 4. Loading frequencies and dynamic moduli calculated in thick and thin AC layer

AC thickness (cm)	Temperature	Layers properties	SMA13	Sup20	Sup25
26	5°C	Loading frequency (Hz)	44.3	12.5	6
		Dynamic modulus (Mpa)	11126.7	9201.3	8103.8
	25°C	Loading frequency (Hz)	44.3	15.9	8.2
		Dynamic modulus (Mpa)	4057	3045.2	2490.2
	50°C	Loading frequency (Hz)	44.3	21.4	12.2
		Dynamic modulus (Mpa)	860.9	654.6	527.7
10	5°C	Loading frequency (Hz)	44.3	9.6	-
		Dynamic modulus (Mpa)	11126.7	8804	-
	25°C	Loading frequency (Hz)	44.3	12.6	-
		Dynamic modulus (Mpa)	4057	2839	-
	50°C	Loading frequency (Hz)	44.3	17.7	-
		Dynamic modulus (Mpa)	860.9	607	-

Table 5. Temperature effect on horizontal strains and locations in pavements with CTB and GB

Base layer	Speed (km/h)	Temperature (°C)	Thick AC layer		Thin AC layer	
			ε_x (Top) (μstrain)	ε_y (Bottom (μstrain)	ε_x (Top) (μstrain)	ε_y (Bottom (μstrain)
CTB	8	5	16.6	5.9	4.8	2.6
		25	94.7	-4.6	63.5	-16.5
		50	635.1	-13.9	516.6	-26.6
	120	5	8.1	8.2	-0.3	7.5
		25	35.3	2	17.6	-4.9
		50	212.3	-9.5	160.1	-23.1
GB	8	5	6.5	111.2	26.1	204.9
		25	23.6	225.8	58.3	364
		50	459.8	318.1	431.4	432.8
	120	5	2.4	81.6	19.6	159
		25	12.9	154.3	36.9	268.6
		50	92.9	282.4	118.3	427.4

882

883

884

885 Table 6. Speed variations effect on critical horizontal strains in thick and thin pavements with CTB
886 layer

Speed (km/h)	Pavement structure	5°C		25°C		50°C	
		ε_x^* (Top)	ε_y^* (Bottom	ε_x^* (Top)	ε_y^* (Bottom	ε_x^* (Top)	ε_y^* (Bottom
8	Thick	16.6	5.9	94.7	-4.6	635.1	-13.9
	Thin	4.8	2.6	63.5	-16.5	516.6	-26.6
24	Thick	12.2	7.1	62.6	-1.8	408.5	-12.5
	Thin	2	5	38.1	-11.7	324.8	-25.5
48	Thick	10.2	7.6	48.6	-0.1	308.5	-11.4
	Thin	0.9	6.2	27.4	-8.6	240.7	-24.6
72	Thick	9.2	7.9	42.1	0.8	261.9	-10.6
	Thin	0.4	6.8	22.5	-6.9	201.6	-23.9
96	Thick	8.5	8.1	38.1	1.5	233	-10
	Thin	-0.1	7.2	19.4	-5.7	177.7	-23.5
120	Thick	8.1	8.2	35.3	1.9	212.3	-9.5
	Thin	-0.2	7.5	17.6	-4.9	160.1	-23.2

887 *Strain values at the top and bottom of AC layers are in microstrains.

888

889

890

891

892

893

894

895

896

897

898

899

Table 7. Speed variations effect on critical horizontal strains in thick and thin pavements with GB layer

Speed (km/h)	Pavement structure	5°C		25°C		50°C	
		ε_x^* (Top)	ε_y^* (Bottom	ε_x^* (Top)	ε_y^* (Bottom	ε_x^* (Top)	ε_y^* (Bottom
8	Thick	6.5	111.2	23.7	225.8	459.8	318.1
	Thin	26	204.9	58	364	431.4	432.8
24	Thick	4.5	97	18.9	194.5	257.4	311.7
	Thin	23	183	47.7	324.1	252.2	444.4
48	Thick	3.5	89.8	16.2	176.2	171.6	301.4
	Thin	21.5	171.7	42.3	299.1	186.4	442
72	Thick	3	85.9	14.7	166.1	133	293.8
	Thin	20.7	165.7	40	285.2	153.8	436.9
96	Thick	2.6	83.4	13.64	159.3	109.7	287.6
	Thin	20	161.6	38.3	275.9	133.3	432
120	Thick	2.4	81.6	12.9	154.3	92.95	282.4
	Thin	19.6	159	36.9	268.6	118.3	427.4

*Strain values at the top and bottom of AC layers are in microstrains.